

# TEM studies of strain-induced martensitic formation in fatigued Fe-18Mn alloy

S. C. TJONG, C. C. HUNG, N. J. HO

*Institute of Materials Science and Engineering, National Sun Yat-Sen University, Kaohsiung, Taiwan*

Austenitic Fe-18Mn alloy was cyclically deformed at various total strain amplitudes. The structural changes induced by cyclic straining in Fe-18Mn alloy were investigated by transmission electron microscopy. At a low strain amplitude of 0.4%, the formation of  $\varepsilon$ -martensite associated with deformation twins and stacking faults was observed in this alloy. As the applied strain amplitude was increased to 1.0%,  $\alpha'$ -martensite embryos were induced in the alloy investigated. These embryos coalesce into a lath structure upon subsequent cyclic deformation.

## 1. Introduction

High-manganese steels have received considerable attention recently for a variety of applications. Binary Fe-Mn alloys normally contain a manganese content above 16 wt%. Manganese is well known as an austenite-stabilizing element, and the addition of manganese to iron-base alloys allows manganese to replace critical alloying elements such as nickel and chromium. Like chromium it stabilizes the austenite phase in high-manganese alloys, and also improves the corrosion resistance in amounts above 12% [1]. The Fe-Mn alloys are considered of practical interest for use in very low temperature service. For cryogenic applications, these austenitic alloys are used as the materials for the magnet case of a fusion reactor [1]. The alloys in the magnet case must possess good combinations of strength, toughness and fatigue resistance [1]. The microstructure and toughness of iron-high-manganese alloys have been investigated by Morris *et al.* [2]. They reported that intergranular failure was a predominant fracture mode in high-manganese steels [2]. On the other hand, much less work has been done on the low-cycle fatigue behaviour of Fe-Mn alloys. The Fe-18.5 wt% Mn alloys also exhibits a shape memory effect governed by the  $\gamma \rightleftharpoons \varepsilon$  martensitic transformation [3]. The shape memory alloys are used in applications such as pipe and tube couplings and electronic tight seals and connectors.

It has been observed that the austenitic stainless steels undergo transformation to  $\varepsilon$ - and  $\alpha'$ -martensites on being plastically deformed. The martensitic transformation can be induced by the application of stress and plastic strain. The influence of the stress state on transformation has received considerable attention. Patel and Cohen [4] showed that the shear component of the applied stress assists the martensitic transformation. The normal stress component may be aided or opposed depending whether it is tensile or compressive [4]. Stress-induced martensite has been observed

in Fe-18Cr-14Ni alloy and Fe-30Mn-1Si alloy by Sato and co-workers [5, 6]. They reported that the shear stress acting on  $\langle \bar{1}120 \rangle_{\varepsilon} \{ \bar{1}100 \}_{\varepsilon}$  initiates the  $\varepsilon \rightarrow \alpha'$  transformation. Recently, Tomota *et al.* [7] have observed the stress-induced  $\varepsilon \rightarrow \alpha'$  transformation in binary iron-high-manganese alloys. They showed that the  $\alpha'$ -martensite formed from the earliest stages of deformation was quite effective in decreasing the work-hardening rate. However, the accumulation of  $\alpha'$ -martensite during the later stage of deformation resulted in an increase of the work-hardening. At this later stage, the  $\alpha'$ -martensite becomes an obstacle to succeeding plastic deformation [7]. Maxwell *et al.* [8] have conducted a metallographic study on stress-assisted and strain-induced martensites in Fe-Ni-C alloys. They indicate that the morphology of the stress-assisted martensite was identical with that of the unstressed plate martensite formed by cooling below the transformation temperature. On the other hand, the strain-induced martensite was formed along the slip bands of the austenite as fine parallel laths.

In strain-induced transformations, plastic deformation of the parent phase creates a defect structure which acts as a nucleation site for the transformation product. The strain-induced martensite that forms in 300-series austenitic stainless steels is either bcc  $\alpha'$ -martensite, hcp  $\varepsilon$ -martensite or a mixture of the two. The amount of  $\alpha'$ -martensite formed in 304 stainless steel depends on various conditions of strain, strain rate and strain state. Olson and Cohen [9] have reported that the interactions of shear band bands in 304 stainless steel are the effective sites for the nucleation of strain-induced  $\alpha'$ -martensite. The shear bands include martensite, mechanical twins and dense bundles of stacking faults. The volume fraction of  $\alpha'$ -martensite is a sigmoidal function of plastic strain. Early work by Powell *et al.* [10] showed that the amount of martensite decreased with increasing strain rate. The increased stability of austenite resulted from adiabatic heating during high-rate deformation. The

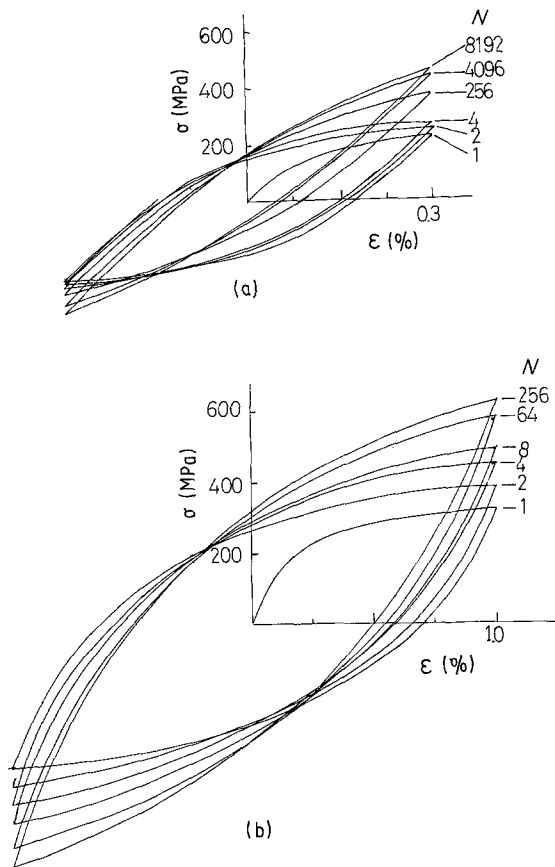


Figure 1 Hysteresis loops for Fe-18Mn alloy at applied strain amplitudes of (a) 0.3% and (b) 1.0%.

tendency for the formation of  $\alpha'$ -martensite increased with a change of strain state from uniaxial toward biaxial or triaxial. Murr *et al.* [11] reported that biaxial tension was more effective in forming  $\alpha'$  martensite than uniaxial tension. This was because the biaxial tension tended to produce more shear bands and intersections than uniaxial tension. Recently, Johnson *et al.* [12] reported that a large volume fraction (exceeding 70%) of  $\alpha'$ -martensite was induced in

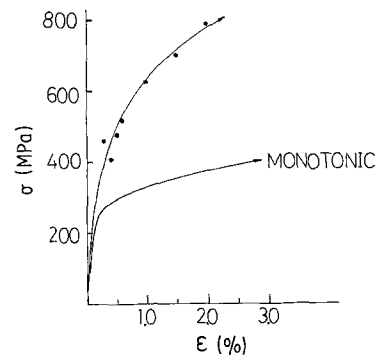


Figure 2 Monotonic and cyclic stress-strain curves for the Fe-18Mn alloy.

304 stainless steel shock-deformed in a cylindrical geometry which involved a triaxial state.

The mechanisms of the  $\gamma \rightarrow \alpha'$  transformation in austenitic stainless steels are still unclear and being disrupted. The transformation may proceed as a sequence with the  $\epsilon$ -martensite acting as an intermediate phase. However, several workers have shown that the  $\gamma \rightarrow \alpha'$  transformation can also proceed without going through the  $\epsilon$  phase [9, 13]. This paper reports the results of an examination by transmission electron microscopy (TEM) of the structural changes induced by fatigue in Fe-18Mn alloy at room temperature.

## 2. Experimental procedure

The Fe-18Mn alloy (where the composition is in weight per cent) was prepared by melting high-purity iron and manganese in a laboratory induction furnace. It was then cast into a steel mould. The cast ingot was hot-forged at 1200°C into a billet. This billet was homogenized at 1100°C for 43.3 ksec and subsequently hot-rolled to plates of 12.7 mm thickness.

Before machining, the alloy investigated was further solution-treated at 1200°C for 7200 sec to eliminate

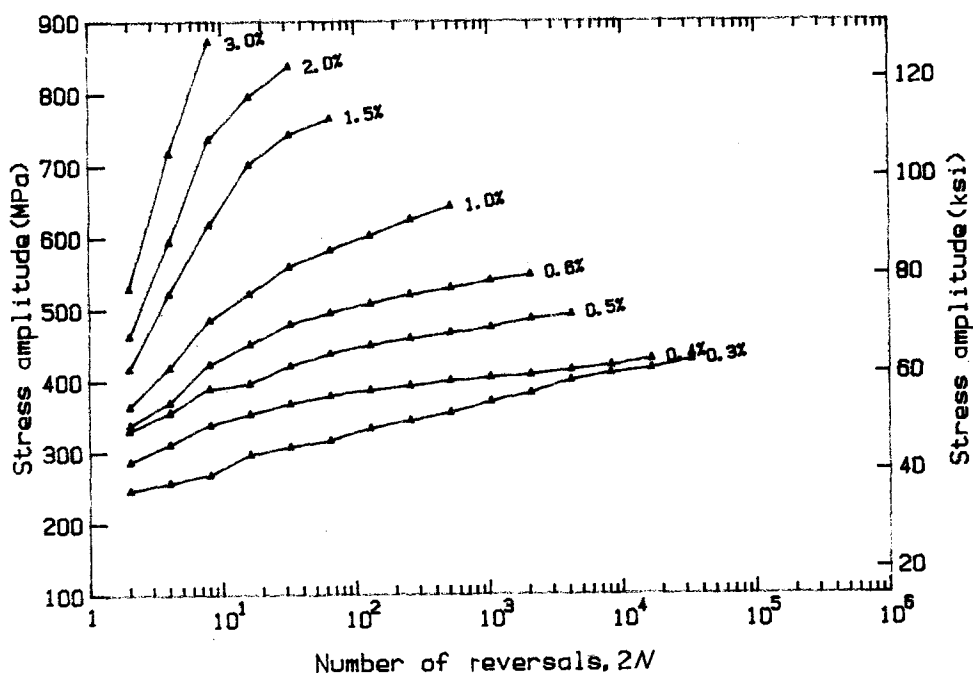


Figure 3 Cyclic stress responses against number of reversals for austenitic Fe-18Mn alloy.

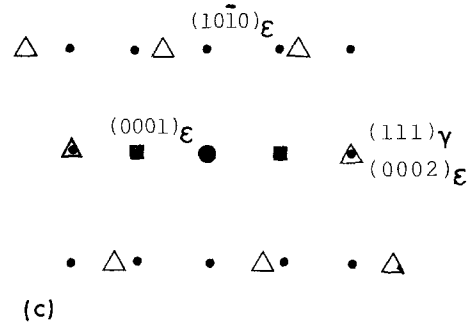
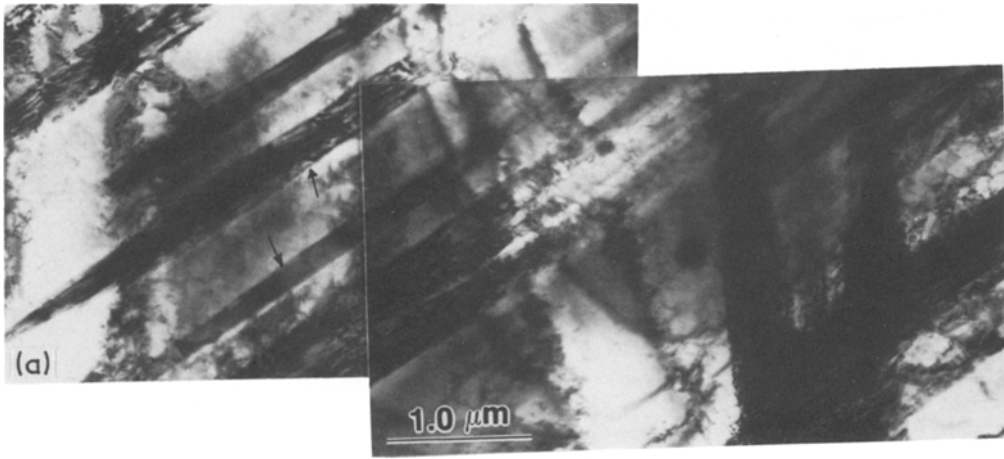


Figure 4 (a) Bright-field TEM micrograph showing the development and growth of  $\epsilon$ -martensite from stacking faults. (b) Selected-area diffraction pattern and (c) indexed diagram: ( $\Delta$ )  $\gamma$ ,  $[01\bar{1}]$ ; ( $\bullet$ )  $\epsilon$ ,  $[21\bar{1}0]$ ; ( $\blacksquare$ )  $\epsilon$ , double diffraction.

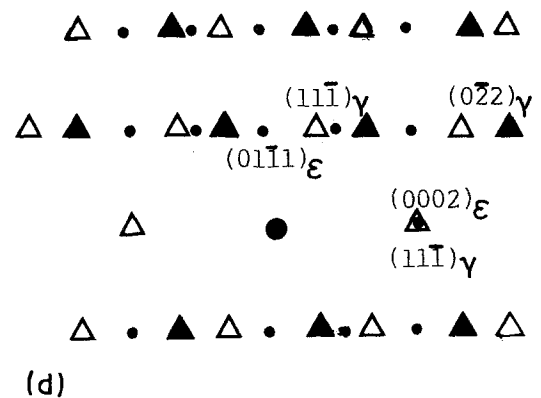
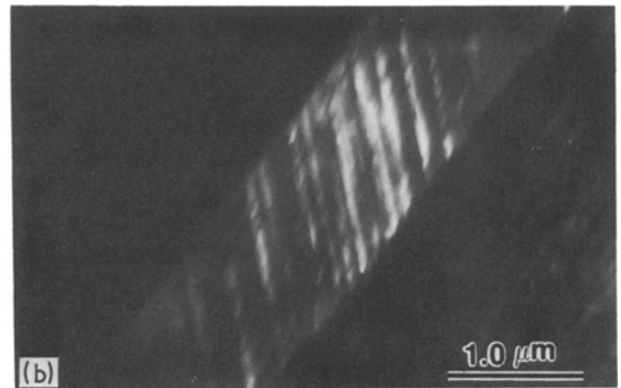
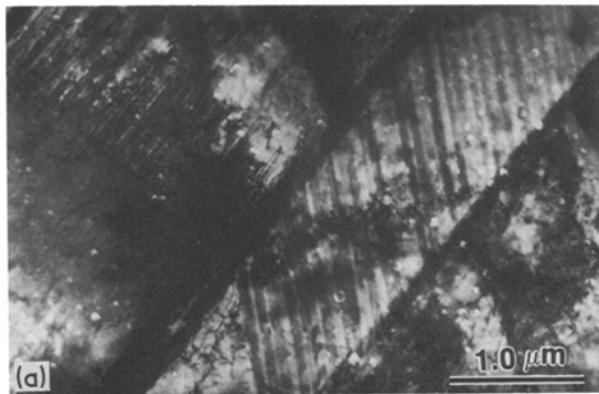


Figure 5 (a) Bright-field electron micrograph showing the formation of  $\epsilon$ -martensite associated with the deformation twins. (b) Dark-field electron micrograph. (c) Selected-area diffraction pattern and (d) indexed diagram: ( $\bullet$ )  $\epsilon$ ,  $[1\bar{2}10]$ ; ( $\Delta$ )  $\gamma$ ,  $[01\bar{1}]$ ; ( $\blacktriangle$ )  $\gamma$ , twin reflection.

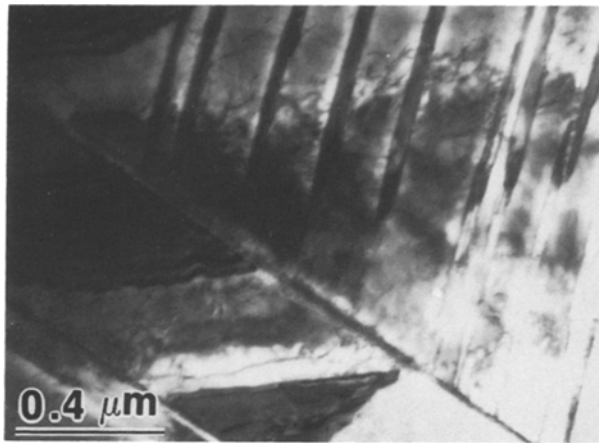


Figure 6 TEM micrograph showing the presence of  $\epsilon$ -martensite platelets in the Fe-18Mn alloy fatigued at 0.6% total strain amplitude.

any hot-rolling effects. The fatigue specimens were then machined from the plates with the specimen axis parallel to the direction of rolling. The room-temperature mechanical properties of the Fe-18Mn alloy are listed in Table I

Fatigue tests were conducted at room temperature in the fully reversed strain-controlled mode using an Instron Model 1332 closed-loop servohydraulic testing machine. A clip-on extensometer of 10.0 mm gauge length was used to measure and control the strain. Sine-wave strain signals were employed at test frequencies varying from 0.05 to 1 Hz. Low melting point Wood's metal grips were used to aid in alignment. Stress-strain hysteresis loops were plotted on an X-Y recorder.

After fatigue testing, the specimens were sectioned beneath the fracture surface for TEM studies. The TEM specimens were prepared by cutting thin foils from the gauge length of the fatigued specimens with a slow diamond saw with an oil lubricant. Disc specimens of 3 mm diameter were punched out and thinned using a twin-jet electropolisher with a solution of 10% perchloric acid and 90% acetic acid. The TEM observations were made on a Jeol Model JEM-200CX scanning transmission electron microscope.

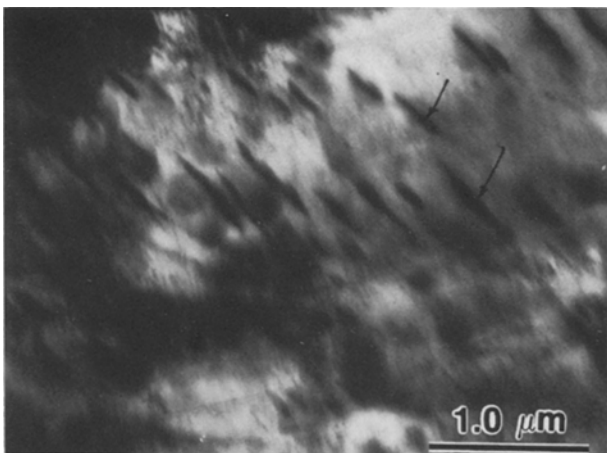


Figure 7 TEM micrograph of Fe-18Mn alloy cycled at 1.0% showing deformation-induced  $\alpha'$ -martensitic embryos.

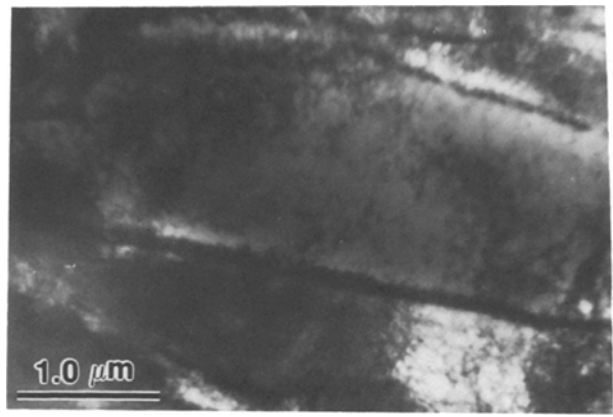


Figure 8 Bright-field electron micrograph showing the dislocated  $\alpha'$ -martensite laths in Fe-18Mn alloy fatigued at 1.5% total strain amplitude.

### 3. Results and discussion

Figs 1a and 1b show representative shapes of the hysteresis loops of Fe-18Mn alloy cycled at total strain amplitudes of 0.3 and 1.0%, respectively. The monotonic true stress against true strain curve for the Fe-18Mn alloy at room temperature taken from the first quarter-cycle of the cycle hysteresis loops is plotted in Fig. 2. The alloy investigated experiences rapid cyclic hardening characteristics as the applied strain amplitude is increased to 0.8%. Plots of the stress amplitude against reversals to failure of this alloy tested at various strain amplitudes are shown in Fig. 3. One can see that the Fe-18Mn alloy exhibits cyclic hardening behaviour from low to high strain amplitudes.

Fig. 4a shows a bright-field electron micrograph of the Fe-18Mn alloy cycled at a total strain amplitude of 0.4%. This micrograph shows the development and growth of  $\epsilon$ -martensite from the stacking faults. It is apparent that very thin bands of  $\epsilon$ -martensite as indicated by the arrows are also observed at this stage; some of them can be seen to contain stacking faults. Gartstein and Rabinkin [14] reported that dislocations in the austenitic matrix dissociate upon deformation, owing to the low value of the stacking fault energy. The interaction of dissociating dislocations leads to the formation of small and wide stacking faults. These stacking faults act as the embryos for the martensitic transformation [14]. Tomota *et al.* [7] reported that is Shockley partial dislocations form and extend on every other layer in the  $\gamma$  phase, the stacking faults would be piled up to form  $\epsilon$ -martensite. In this work, the interactions of dissociating dislocations leading to the formation of wide stacking faults can be seen in the lower right-hand side of Fig. 4b. A selected-area diffraction pattern of this  $\gamma \rightarrow \epsilon$  transformation is shown in Fig. 4b. The orientation relationship as shown in Fig. 4b is typically  $[01\bar{1}]_{\gamma} \parallel [21\bar{1}]_{\epsilon}$ , which

TABLE I Room-temperature mechanical properties of the Fe-18Mn alloy

Modulus of elasticity	147 GPa
0.2% offset yield strength	222 MPa
Ultimate tensile strength	890 MPa
Elongation	24%
Reduction in area	17.5%

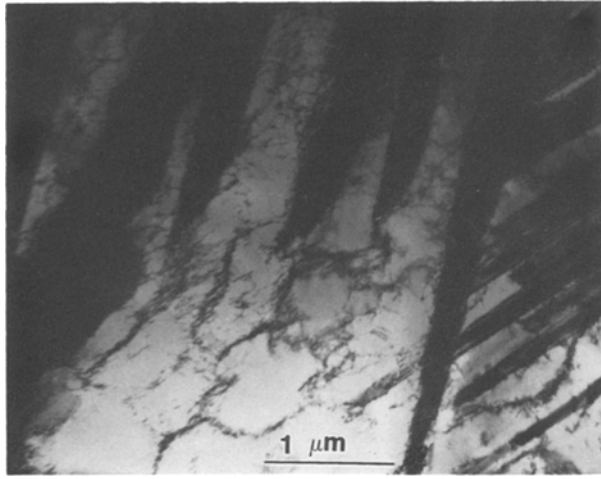


Figure 9 TEM micrograph showing formation of cell structure in the faulted austenitic matrix of Fe-21Mn-2.5Al alloy fatigued at a total strain amplitude of 1.0% (from Tjong and Ho [21]).

is similar to that reported by other workers [14]. It has been reported by Olson and Cohen [15] that an hcp martensite which obeys the  $[1\bar{1}0]_y \parallel [11\bar{2}0]_x$  orientation relationship can be created from the fcc lattice by the passage of a Shockley partial dislocation on every second closed packing plane. The first step in the martensitic nucleation process is faulting on planes of closest packing [15]. Morris *et al.* [16] showed both  $\epsilon$ -martensite and deformation twins were formed in Fe-Mn alloys after monotonic straining. Periodic twinning on the basal plane in the fcc structure leads to the nucleation of  $\epsilon$ -martensite. Previous studies [17, 18] have shown twinning to be a common deformation mechanism for mechanically strained fcc single-crystal thin films. Rigsbee and Benson [19] have indicated that the presence of hydrogen in 304 stainless steel after cathodic charging can result in the formation of deformation twins and  $\epsilon$ -martensite. In the present work, bright- and dark-field electron micrographs showing the formation of  $\epsilon$ -martensite associated with deformation twins are shown in Figs 5a and b, respectively. The corresponding electron diffraction pattern and indexed diagram are shown in Figs 5c and d, respectively. One can see from the dark-field micrograph that the  $\epsilon$ -martensite plate consists of deformation twins, and these twins are evenly distributed. As the applied strain is increased to

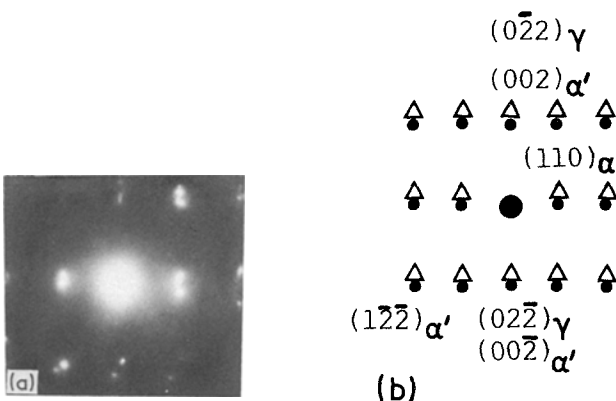


Figure 10 (a) Selected-area diffraction pattern of  $\alpha'$ -martensite laths as shown in Fig. 8. (b) Indexed diagram: (●)  $\gamma$ ,  $[211]_y$ ; (▲)  $\alpha'$ ,  $[110]_x$ .

0.6%, the microstructure of the alloy investigated consists of  $\epsilon$ -martensite platelets along with few dislocations in the retained austenitic matrix (Fig. 6).

Fig. 7 shows a bright-field TEM micrograph of the Fe-18Mn alloy cycled at a strain amplitude of 1.0%. It is apparent from the micrograph that  $\alpha'$ -martensite embryos as indicated by the arrows were induced in the Fe-18Mn alloy. These embryos seem to have a long disc structure. The embryos may coalesce into a lath structure upon subsequent cyclic deformation or when the applied strain is further increased. Murr *et al.* [11] reported that repeated nucleation, coalescence and growth of  $\alpha'$  embryos during biaxial tension of 304 stainless steel resulted in the formation of  $\alpha'$ -martensite laths. The nucleation of  $\alpha'$ -martensite embryos in the austenitic matrix of Fe-18Mn alloy leads to an increase in the hardening rate as shown in Fig. 3

Fig. 8 shows two parallel  $\alpha'$ -martensite laths in Fe-18Mn alloy cycled at a strain amplitude of 1.5%. Dislocations are seen within the laths with no evidence of any  $\epsilon$ -martensite or twinning. In general, the  $\alpha'$ -martensite laths are found to consist of a high density of tangled dislocations as has been reported by Wakasa and Wayman [20]. In the case of Fe-18Mn alloy, we did not observe the presence of cell structure when cycled at a strain amplitude of 1%. However, cell structure,  $\epsilon$ - and  $\alpha'$ -martensites (Fig. 9) were observed in Fe-21Mn alloy containing 2.5% Al addition in a previous study [21]. It was suggested that the addition of aluminium to Fe-21Mn alloy affects the stacking-fault energy of the alloy, as stacking-fault energy directly influences the ease of cross-slip. Alloys having a low stacking-fault energy tend to produce coplanar arrays of dislocations, whereas a high stacking-fault energy gives rise to cell structure after a stress corrosion cracking test [22]. Degallaix *et al.* [23] also indicated that cyclic deformation of an austenitic alloy with a low stacking-fault energy generally leads to the formation of planar arrays of dislocations instead of cell structure at higher applied strain amplitudes. Fig. 10a shows the selected-area diffraction pattern of martensite laths as indicated in Fig. 8, and Fig. 10b shows the corresponding indexed diagram. As can be seen in Fig. 10, the orientation between the austenite and  $\alpha'$ -martensite is  $[211]_y \parallel [110]_x$ . This orientation obeys the Nishiyama relation. The relative orientation of the austenite and  $\alpha'$ -martensite obeys either the Bain, the Kurdjumov-Sachs or the Nishiyama relation [24, 25]. Recently, Tjong and Ho [21] reported that the relative orientation of the strain-induced  $\alpha'$ -martensite and austenite in Fe-21Mn-2.5Al alloy obeys the Nishiyama relation [21].

#### 4. Conclusion

The microstructure of Fe-18Mn alloy cycled at a low strain amplitude of 0.4% consists of deformation twins and stacking faults. However, as the applied strain amplitude is increased to 1.0% the microstructure consists of  $\alpha'$ -martensite embryos. With further increase of the strain amplitude to 1%,  $\alpha'$ -martensite laths were observed in this alloy.

## References

1. J. W. MORRIS Jr and E. N. C. DALDER, in "Selection of Materials for Service Environments", edited by H. E. Boyer (American Society for Metals, Ohio, 1984) p. 274.
2. Y. TOMOTA, M. STRUM and J. W. MORRIS Jr, *Metall. Trans. A* **18A** (1987) 1073.
3. K. ENAMI, A. NAGASAWA and S. NENNO, *Scripta Metall.* **27** (1976) 1053.
4. J. R. PATEL and M. COHEN, *Acta Metall.* **1** (1953) 531.
5. A. SATO, H. KASUGA and T. MORI, *ibid.* **28** (1980) 1223.
6. A. SATO, K. SOMA and T. MORI, *ibid.* **30** (1982) 1901.
7. Y. TOMOTA, M. STRUM and J. W. MORRIS Jr, *Metall. Trans. A* **17A** (1986) 537.
8. P. C. MAXWELL, A. GOLDBERG and J. C. SHYNE, *Metall. Trans.* **5** (1974) 1305.
9. G. B. OLSON and M. COHEN, *Metall. Trans. A* **6A** (1975) 791.
10. G. W. POWELL, E. R. MARSHALL and W. A. BACKOFEN, *Trans. ASM* **50** (1958) 479.
11. L. E. MURR, K. P. STAUDHAMMER and S. S. HECKER, *Metall. Trans. A* **13A** (1982) 627.
12. K. A. JOHNSON, L. E. MURR and K. P. STAUDHAMMER, *Acta Metall.* **33** (1985) 677.
13. T. SUZUKI, H. KOZIMA, K. SUZUKI, T. HASHIMOTO and I. ICHIHARA, *ibid.* **25** (1977) 1151.
14. E. GARTSTEIN and A. RABINKIN, *ibid.* **27** (1979) 1053.
15. G. B. OLSON and M. COHEN, *Metall. Trans. A* **7A** (1976) 1897.
16. J. W. MORRIS Jr, S. K. HWANG, K. A. YUSHCHENKO, V. T. BELOTZERKOVERTZ and O. G. KVASNEVSKII, *Adv. Cry. Eng.* **24** (1978) 91.
17. J. W. MATTHEWS, *Acta Metall.* **18** (1970) 175.
18. R. E. WINTER and J. E. FIELD, *Phil. Mag.* **29** (1974) 395.
19. J. M. RIGSBEE and R. B. BENSON Jr, *J. Mater. Sci.* **12** (1977) 406.
20. K. WAKASA and C. M. WAYMAN, *Acta Metall.* **29** (1981) 991.
21. S. C. TJONG and N. J. HO, *Mater. Sci. Eng.* **A102** (1988) 125.
22. D. L. DOUGLASS, G. THOMAS and W. R. ROSER, *Corrosion* **20** (1964) 15.
23. S. DEGALLAIX, J. FOCT and A. HENRY, *Mater. Sci. Technol.* **2** (1986) 946.
24. G. THOMAS, *Metall. Trans. A*, **9A** (1978) 439.
25. B. V. N. RAO, *ibid.* **10A** (1979) 645.

Received 11 December 1987

and accepted 6 May 1988